



HAL
open science

Stimulation of Geothermal Reservoirs: Impedance and Efficiency of Thermal Recovery

Murad S. Abuaisha, Benjamin Loret

► **To cite this version:**

Murad S. Abuaisha, Benjamin Loret. Stimulation of Geothermal Reservoirs: Impedance and Efficiency of Thermal Recovery. 40th Workshop on Geothermal Reservoir Engineering, Jan 2015, Stanford, CA, United States. hal-02460721

HAL Id: hal-02460721

<https://minesparis-psl.hal.science/hal-02460721>

Submitted on 30 Jan 2020

HAL is a multi-disciplinary open access archive for the deposit and dissemination of scientific research documents, whether they are published or not. The documents may come from teaching and research institutions in France or abroad, or from public or private research centers.

L'archive ouverte pluridisciplinaire **HAL**, est destinée au dépôt et à la diffusion de documents scientifiques de niveau recherche, publiés ou non, émanant des établissements d'enseignement et de recherche français ou étrangers, des laboratoires publics ou privés.

Stimulation of Geothermal Reservoirs: Impedance and Efficiency of Thermal Recovery

Murad Abuaisha, Benjamin Loret

► **To cite this version:**

Murad Abuaisha, Benjamin Loret. Stimulation of Geothermal Reservoirs: Impedance and Efficiency of Thermal Recovery. 40 th Annual Stanford Geothermal Workshop, Jan 2015, Stanford, United States. hal-02460721

HAL Id: hal-02460721

<https://hal-mines-paristech.archives-ouvertes.fr/hal-02460721>

Submitted on 30 Jan 2020

HAL is a multi-disciplinary open access archive for the deposit and dissemination of scientific research documents, whether they are published or not. The documents may come from teaching and research institutions in France or abroad, or from public or private research centers.

L'archive ouverte pluridisciplinaire **HAL**, est destinée au dépôt et à la diffusion de documents scientifiques de niveau recherche, publiés ou non, émanant des établissements d'enseignement et de recherche français ou étrangers, des laboratoires publics ou privés.

Stimulation of Geothermal Reservoirs: Impedance and Efficiency of Thermal Recovery

Murad AbuAisha¹ and Benjamin Loret²

1: Université de Grenoble, France, 2: Université de Grenoble, France

1: morad_77_2@hotmail.com 2: Benjamin.Loret@grenoble-inp.fr

Keywords: hydraulic fracturing, thermo-poroelastic framework, viscosity-temperature change, impedance and efficiency

ABSTRACT

The natural permeability of geothermal reservoirs is low and needs to be enhanced to ensure an efficient use and economic viability. Hydraulic fracturing is the standard technique used for that purpose. Impedance and efficiency are key characteristics in regard to the economic viability of geothermal sites.

The influence of hydraulic fracturing process on the efficiency of thermal recovery from Hot Dry Rock (HDR) reservoirs is addressed in a thermo-poroelastic framework. A fracturing model is integrated into a domestic Fortran 90 finite element code that solves transient thermo-poroelastic boundary value problems. The model governs the evolution of the cracks, namely their directions, lengths and apertures. While hydraulic fracturing improves significantly the permeability of the reservoir, and decreases its impedance, it also reduces its life time.

The model parameters are extracted from data on the pilot reservoir at Soultz-sous-Forêts or back-calculated from the stimulations and circulation tests that have been run in 1993, 1997 and 2002-2005. The temperature dependence of the viscosity of the working fluid is shown to affect fluid and heat transports in the poroelastic medium and hence to decrease the efficiency of hydraulic fracturing. Increasing the salt concentration of the brine has comparable effects.

1. INTRODUCTION

Thermal recovery from Hot Dry Rock (HDR) reservoirs is seen as an alternative to grey energies. Thermal extraction from geothermal systems is achieved by injecting cold fluids into deep reservoirs where the temperature gradient is favorable. The economic viability of the recovery process is controlled by crucial factors which should be scrutinized. Such factors include, inter alia, the development of the reservoir pressure, of effective stresses and fluid losses, Bruel [1995]_{1,2}. Damage, permeability change and irreversible processes may also play a significant role in the overall behavior of the HDR reservoirs. Modern geothermal projects are nowadays focusing on enhancing the permeability of the geothermal reservoirs, Enhanced Geothermal Systems (EGS). Geothermal fluids are injected with such high flow rates that the assumption of time-independent permeability is entirely improper. Extreme thermo-poroelastic changes are expected to take place near the injection well. Indeed, such abrupt changes, at certain injection rates, will cause fractures to evolve and to connect and permeability to increase in a highly heterogeneous manner, AbuAisha [2014]. The increase in HDR reservoir permeability due to Hydraulic Fracturing (HF) is bound to affect the thermal recovery process significantly.

Hydraulic fracturing in a thermo-poroelastic framework has been presented in AbuAisha [2014]. The direction of the flow and the generation of the new hydraulically created fracture networks may take place within the entire reservoir volume. As a key ingredient of the framework, a simple Hydraulic Fracturing Model (HFM) based on an opening mode of fracture evolution (Mode I), associated with a normal discontinuity of the displacement field, is used in a first step. The HFM is capable of tracking the fracture evolution in all possible directional orientations at any geometrical point. The updated fracture properties namely, fracture radius and aperture, are used to calculate an anisotropic permeability tensor which describes the hydraulic connectivity of the fractured medium. The basic HFM has been subsequently modified so as to quantify the influence of the mechanical details on the overall performance of the EGS.

The HFMs are used to simulate circulation tests between an injection well and two production wells in a simplified geometrical setting. Field data from several references are collected to validate the numerical simulations. The effects of HF on the designing characteristics of HDR reservoirs, i.e. impedance and efficiency, are addressed. The field record of the Soultz-sous-Forêts geothermal site presented in Bruel [1995]₂ has proven that HF affects significantly the efficiency of thermal extraction process. The size of HDR reservoirs to ensure efficient thermal extraction and long-term low impedance has been discussed by Jupe et al. [1995].

The model is thought to be adapted to the enhancement of geothermal systems. In fact, hydraulic fracturing has also been used for years to enhance recovery of oil and gas. However, the technique, and henceforth the modeling, is specialized to each domain. For heat recovery from geothermal reservoirs, a few key points should be emphasized:

- at variance with hydraulic fracturing in a petroleum engineering context, the length over which the permeability should be enhanced encompasses several hundred meters. The initial heterogeneities due to pre-existing faults certainly attract and modify the enhancement that would develop in an otherwise homogeneous formation. Re-activation of these faults alone is to be avoided as the process would easily produce shortcuts and render the circulation paths inefficient. Therefore, even if spatial heterogeneities of the enhanced permeability are unavoidable, a significant piece of volume where the fracture network can be considered as homogeneously stimulated should be sought;

- modeling of hydraulic fracturing in petroleum engineering in a finite element context insists on creating a few fractures, typically extending over a borehole diameter, from existing singularities around the well using numerical enhanced strain or pressure fields and cohesive crack tips. Such an approach is not viable in a geothermal context: indeed, as already indicated, a) the fracture network should be much more homogeneously spread; b) the length scale is orders of magnitude larger; and c) critically, the width of the fractures is of capital importance for the permeability.

This last point, namely the width of the extended cracks, is boldly ignored by most, if not all, current finite element methods which put emphasis on the length of the extension of the discrete cracks and on their direction. While these features are also important in our approach, it turns out that the width of the crack is a key factor that controls the evolution of the permeability.

This work is aimed at studying the effect of HF on the impedance and efficiency of HDR reservoirs using finite element simulations which are correlated to field data when available. It also discusses the effect of temperature change on the viscosity of brines used in running geothermal systems, and the subsequent implications on the HF process and hence impedance and efficiency. The fracturing models with and without a temperature dependent viscosity are implemented in a domestic Fortran 90 finite element code and the simulations, for the same reservoir, are systematically compared. Some considerations to help designing an appropriate time course of injection pressure or flow rate are included as well as issues pertaining to the stability of the wellbores.

2. HYDRAULIC FRACTURING MODEL (HFM)

This section provides the basic elements of a fracturing model which is capable of ensuring a directionally stable mode I of fracture evolution.

2.1 Fracturing criterion

Let us consider a group of fractures of average radius r and arbitrary normal direction \mathbf{n} in the horizontal plane (x, y) around a vertical borehole. If the borehole pressure is gradually increased to a point the normal effective stress $\sigma'_n = \mathbf{n} \cdot \boldsymbol{\sigma}' \cdot \mathbf{n}$ (at the fracture tip) becomes tensile and exceeds the limit of material tensile strength, the group of fractures starts propagating and consequently the average aperture increases. To track the evolution of the average radius r of a group of fractures in direction \mathbf{n} , a simple criterion is adopted:

$$F(\sigma'_n, r) = f(r) \sigma'_n \sqrt{\pi r} - K_{Ic} = 0 \quad \text{with} \quad f(r) = \eta \begin{cases} r_f/r, & r < r_f \\ 1, & r \geq r_f \end{cases} \quad (1)$$

where K_{Ic} is the toughness of the rock for mode I of fracture. The positive scalar valued function $f(r)$ controls the stability of fracture propagation, with r_f denoting the critical fracture radius for accelerated coalescence of micro-fractures, and η is the fracture growth stabilizing parameter. The fracture aperture w is taken as an increasing power function of the fracture radius r , AbuAisha [2014], Chap. 2.

2.2 Permeability tensor

From the fracture radius $r(\mathbf{n})$ and aperture $w(\mathbf{n})$ of arbitrary direction \mathbf{n} , the local velocity field is calculated by implementing Navier-Stokes equation for laminar flow between two parallel plates. An anisotropic permeability tensor, which is provided by the fractures, is calculated by averaging the individual Poiseuille flows over all the directions of the space, i.e. by integrating over the unit sphere S^2 ,

$$\mathbf{k}_c = \frac{1}{48} \frac{N}{V} \int_{S^2} C(\mathbf{n}) w^3(\mathbf{n}) r^2(\mathbf{n}) (\mathbf{I} - \mathbf{n} \otimes \mathbf{n}) dS \quad \text{with} \quad C(r(\mathbf{n})) = c_c \frac{r(\mathbf{n}) - r_0}{r_f - r_0} \quad (2)$$

where \mathbf{I} is the identity tensor and N/V the fracture density (number of fractures N in the volume V). The connectivity coefficient $C(\mathbf{n})$ indicates that connectivity between fractures increases as the fractures grow in size from an initial radius r_0 to r_f , with c_c being a material constant. The overall permeability tensor of the fractured medium is composed of two parts: the initial permeability tensor denoted as \mathbf{k}_0 due to the initial porosity, and the fracture induced permeability tensor denoted by \mathbf{k}_c . The flows in the two cavities are assumed to take place in parallel and the total permeability tensor of the mixture \mathbf{k} (m^2) is obtained by summation, namely $\mathbf{k} = \mathbf{k}_0 + \mathbf{k}_c$.

2.3 Constitutive and field thermo-poroelastic equations

The mechanical response of a poroelastic medium undergoing thermal changes while in local thermal equilibrium is governed by two constitutive equations. The Biot's effective stress of the mixture $\boldsymbol{\sigma} + \kappa p \mathbf{I}$ expresses in terms of the strain $\boldsymbol{\varepsilon}$ and temperature departure $\theta = T - T_0$ with respect to a reference T_0 as,

$$\boldsymbol{\sigma} + \kappa p \mathbf{I} = 2G\boldsymbol{\varepsilon} + \frac{2G\nu}{1-2\nu} \text{tr} \boldsymbol{\varepsilon} \mathbf{I} - K\alpha_s \theta_s \mathbf{I} \quad (3)$$

where $\boldsymbol{\sigma}$ is the total stress, p the pore fluid pressure, $\text{tr} \boldsymbol{\varepsilon}$ the volumetric strain, G the shear modulus, ν the drained Poisson's ratio, $\kappa = 1 - K/K_s$ the Biot's coefficient, K the drained bulk modulus, K_s the bulk modulus of the solid constituent, α_s the cubical thermal expansion coefficient for the solid, and \mathbf{I} the second order identity tensor. Compressive stresses are counted negative.

The change of the fluid mass content,

$$\zeta = \kappa \operatorname{tr} \boldsymbol{\varepsilon} + \frac{p}{M} - \bar{\alpha} \theta \quad (4)$$

involves mechanical, fluid and thermal contributions, with coefficients, $1/M = \kappa/K'_s + \varphi_0 (1/K_f - 1/K_s)$ and $\bar{\alpha} = \kappa \alpha_s + \varphi_0 (\alpha_f - \alpha_s)$, that feature the cubical thermal expansion coefficient of the fluid α_f , the bulk modulus of the fluid K_f and the reference porosity of the mixture φ_0 . Throughout the paper, the subscripts s and f refer to the solid and fluid constituents respectively.

Two additional constitutive equations are needed to define the transport of the fluid and the transfer of heat. First, the constitutive equation of Darcy that describes the seepage of the fluid through the porous medium relates the apparent fluid flux relative to the solid skeleton \mathbf{j}_f (m/s) to the fluid pressure gradient,

$$\mathbf{j}_f = \varphi_0 (\mathbf{v}_f - \mathbf{v}_s) = -\frac{\mathbf{k}}{\mu} \cdot (\nabla p - \rho_f \mathbf{g}) \quad (5)$$

where \mathbf{k} is the permeability tensor of the mixture, μ is the fluid dynamic viscosity (Pa \times s), ρ_f is the intrinsic fluid density (kg/m³), and $\mathbf{g} = g \mathbf{e}$ with g the gravitational acceleration (m/s²) and \mathbf{e} the unit vertical vector directed downwards. Second, according to Fourier's law of heat conduction, the heat flux \mathbf{q}_θ (W/m) is aligned with the negative of the temperature gradient $\nabla \theta$,

$$\mathbf{q}_\theta = -\chi \nabla \theta \quad (6)$$

The porous medium is in local thermal equilibrium so that the effective thermal conductivity $\chi = (1 - \varphi_0) \chi_s + \varphi_0 \chi_f$ (W/m/K) is obtained by volume averaging over the species. The analysis focuses on the evolving anisotropy of the permeability tensor but it is content to consider an isotropic thermal conductivity of the solid.

The displacement vector, pore pressure and temperature are constraint to satisfy three field equations,

$$\begin{aligned} \nabla \cdot \boldsymbol{\sigma} + \rho \mathbf{g} &= \mathbf{0} && \text{balance of momentum of the wole mixture} \\ \nabla \cdot \mathbf{j}_f + \frac{\partial \zeta}{\partial t} &= 0 && \text{balance of mass of the fluid} \\ \nabla \cdot \mathbf{q}_\theta + \rho c_v \frac{\partial \theta}{\partial t} + \rho_f c_{pf} \mathbf{j}_f \cdot \nabla \theta &= 0 && \text{balance of energy of the wole mixture} \end{aligned} \quad (7)$$

Here $\rho = (1 - \varphi_0) \rho_s + \varphi_0 \rho_f$ is the mass density of the mixture. The heat storage contribution is expressed in terms of the volumetric isochoric heat capacity of the mixture, $\rho c_v = (1 - \varphi_0) \rho_s c_{vs} + \varphi_0 \rho_f c_{vf}$ (J/m³/K), which is obtained by volume averaging over the species. The energy equation features convection of heat due to fluid diffusion through the solid skeleton introduced by the isobaric heat capacity of the fluid $\rho_f c_{pf} = \rho_f c_{vf} + K_f \alpha_f^2 T$. The convective term can by no means be neglected in the context of geothermal reservoirs, so that the equation of balance of energy can not be decoupled from the system of equations and solved independently.

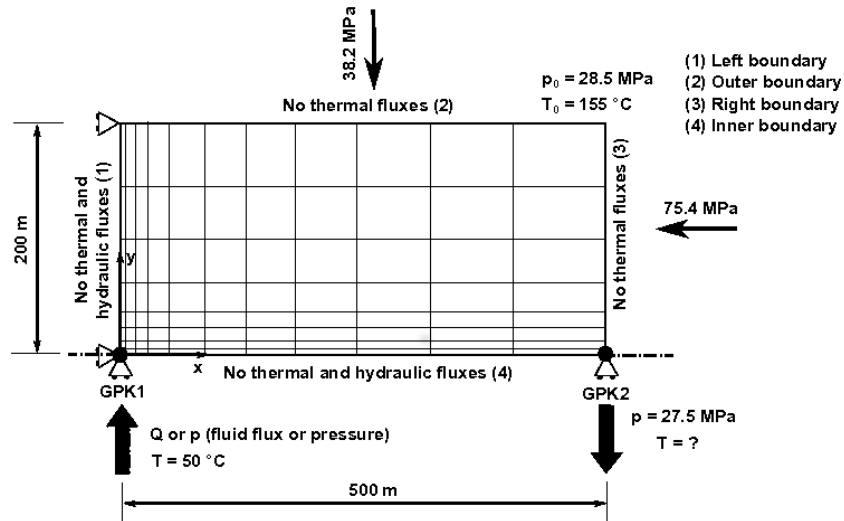


Figure 1: Mesh in the horizontal plane (x, y), initial and boundary conditions used for the stimulation tests at the Soultz-sous-Forêts HDR reservoir, *figure is not to scale*.

3. STIMULATION TESTS OF SOULTZ-SOUS-FORÊTS HDR RESERVOIR

A stimulation test of GPK1 well, between 2800 m and 3500 m, was conducted in 1993 at the Soultz-sous-Forêts HDR reservoir. Pressurized fluid led to fracture evolution which in return generated seismic energy. The works of Bruel [1995]₂ and Jupe et al. [1995] have fairly addressed this stimulation test and shall be used as a guiding reference for our simulations. This section is devoted to define

material data pertaining to the reservoir, the finite element mesh and the initial and boundary conditions. In Section 4, the field flow history at well GPK1 during the stimulation test for 17 days is simulated using the Hydraulic Fracturing Model (HFM) implemented in our domestic finite element code. The time window of the simulations is next extended in Section 5 to study the permeability enhancement of the whole reservoir using the process of HF. The effect of HF on reservoir impedance and efficiency is then highlighted.

Based on the locations of the seismic events presented in Fig. 2 of Bruel [1995]₂ and on the geometrical information provided by Baumgärtner et al. [2000], p. 268, the fractured zone to be stimulated lies at a depth of 2.8 to 2.9 km and has dimensions of 1 km and 400 m around the well GPK1 with N170 Azimuth and W70 Dip. The second well GPK2 is drilled 500 m away from GPK1 and in the direction of fracture evolution (seismic events). The fractured zone to be stimulated is shown in figure 1. The geostatic stresses, the initial pressure p_0 and the initial temperature T_0 correspond to a typical depth of 2.85 km, Bruel [1995]₂, Evans et al. [2009]. The fluid is injected at $T = 50\text{ }^\circ\text{C}$ while the temperature at the outlet production well GPK2 is sought.

Table 1 summarizes the mechanical, hydraulic and thermal boundary conditions used in the stimulation process. The hydraulic boundary conditions will be discussed in Section 4. The conductive heat contribution of the rock formation external to the reservoir domain is secondary for most of the life time of a geothermal reservoir.

Table 1. Boundary conditions for the stimulation tests at Soultz-sous- Forêts:
l=left, r=right, o=outer, and i=inner boundaries of figure 1.

Type	Boundary	Condition
Displacements	l	No horizontal displacement
	i	No vertical displacement
	r and o	Calculated based on the applied stress
Fluid flow	l, i	impermeable
	r and o	Permeable/impermeable
	Injection well	Fluid flux or pressure, figure 2
	Production well	Pore fluid flux pressure ($p=p_0-1\text{MPa}$)
Heat flow	l, i	impermeable
	l, i, r and o	Thermally insulated
	Injection well	$T = 50\text{ }^\circ\text{C}$
	Production well	Temperature is sought

The thermo-poroelastic properties of Soultz-sous-Forêts reservoir are typical for the reservoir rock as shown by Evans et al. [2009]. The value of the initial permeability k_0 has been back-calculated from Fig. 5 of Bruel [1995]₂ by considering that the enhanced permeability of the reservoir has an order of magnitude of $\sim 10^{-11}\text{ m}^2$, Evans et al. [2009]. A mesh of 800 elements, 40 elements in x-direction and 20 elements in y-direction, is used to perform the stimulation. The refinement of the mesh, figure 1, is implemented following two approaches: a) for simulating the logging history at early times, the mesh is refined in x- and y-directions near the injection well to track the strong gradients in its neighborhood; b) for simulating HF over the whole volume of the reservoir, the mesh is to be uniformly spread over the volume.

Table 2. Parameters used in stimulation/HF process.

Type	Parameter	Value	Unit	Ref.
Fracture	Initial radius of fracture r_0	0.25	m	Evans et al.[2009]
	Final radius of fracture r_1	0.80	m	"
	Initial aperture of fracture w_0	3.084×10^{-5}	m	calculated
	Tensile strength T_c	22.8	MPa	calculated
	Compressive strength C_0	228	MPa	Evans et al.[2009]
	Toughness K_{Ic}	1.87	$\text{MPa}\sqrt{\text{m}}$	Atkinson [1991]
	Fracture stabilizing parameter	0.2	-	parameterized
	Fracture density	1×10^6	$1/\text{m}^3$	Bruel [1995] ₂
Flow	Connectivity coefficient c_c	1×10^{-4}	-	Shao et al.[2005]

The rock tensile strength T_c is taken as 10% of rock compressive strength $C_0 = 228\text{ MPa}$. The initial average aperture w_0 is calculated based on the study presented in Chap. 2 of AbuAisha [2014]. The geometrical crack properties, listed in Table 2, will lead to permeability components with maximum magnitude around 10^{-11} m^2 in agreement with Evans et al.[2009], p.79, for the enhanced reservoir. Since the initial permeability of the reservoir k_0 is larger than 10^{-18} m^2 , the excess formation pressure p_w^f needed to start the HF for a temperature change θ of $-105\text{ }^\circ\text{C}$ is found equal to 18 MPa, AbuAisha [2014]. The casing shoe pressure at the injection well

GPK1 should be around $28.5 + 18 = 46.5$ MPa to start hydraulic fracturing. This magnitude is close to the value (around 40 MPa) implemented at Soultz-sous-Forêts to start HF during the field tests at a depth of 2.85 km. The threshold of HF is chosen to be as in the field, namely 40 MPa. The stabilizing parameter η is now determined by equation (1) knowing the effective normal stress σ'_n in the direction of the maximum field stress, the threshold of HF, and the material properties in Table 2.

The shear stability of borehole GPK1 is checked, assuming a friction angle $\vartheta \sim 30^\circ$ and a compressive strength $C_0 = 228$ MPa for granite. The vertical burden stress corresponding to 2.8 km depth is $\sigma_v = \sigma_H = -75.4$ MPa, Evans et al. [2009]. For a failure angle $\beta = \pi/4 + \vartheta/2 \sim 60^\circ$, the minimum value of borehole pressure required to cause shear failure is -0.48 MPa, AbuAisha [2014]. Since the borehole pressure is positive during the HF process, the borehole GPK1 is not likely to fail in shear but rather in tension due to HF.

4. VALIDATION OF THE HFM AT EARLY TIMES OF INJECTION

The reservoir sketched in figure 1 is to be stimulated by the Hydraulic Fracturing Model (HFM) of Section 2. The results of simulations of the HF process are to be correlated with the flow logging injection tests performed at GPK1 well of Soultz-sous-Forêts HDR reservoir in September 1993. The most important level of the stimulation process is located at 2.85 km of GPK1 and absorbs about 60% of the injected fluid.

The field test was implemented by pumping water into GPK1 well gradually until a total flow rate¹ of 40 l/s was reached at day 17. The experimental pressure curve at the injection well showed non- linear relation with injected flow announcing the existence of turbulent flow. Our simulations for the HF process will be performed by following the schemes presented in Table 3.

Table 3. Injection pressure at GPK1 during the 1993 field injection test.

Scheme	Boundary condition at GPK1	Condition at outer and right boundaries
1	Linear flow rate (in 17 days) from 0.13 to 20 l/s	Impermeable boundaries
2	Linear flow rate (in 17 days) from 0.13 to 20 l/s	Permeable boundaries (p=p ₀ =28.5MPa)

Figure 2(left) shows the applied flow rate history at GPK1 well as suggested by the experimental work of Bruel [1995]₂ and as applied in our simulations. Figure 3 displays the response obtained by our HFM, first and second schemes in Table 3, and the experimental data obtained from Fig. 1 of Bruel [1995]₂ for a period of 17 days.

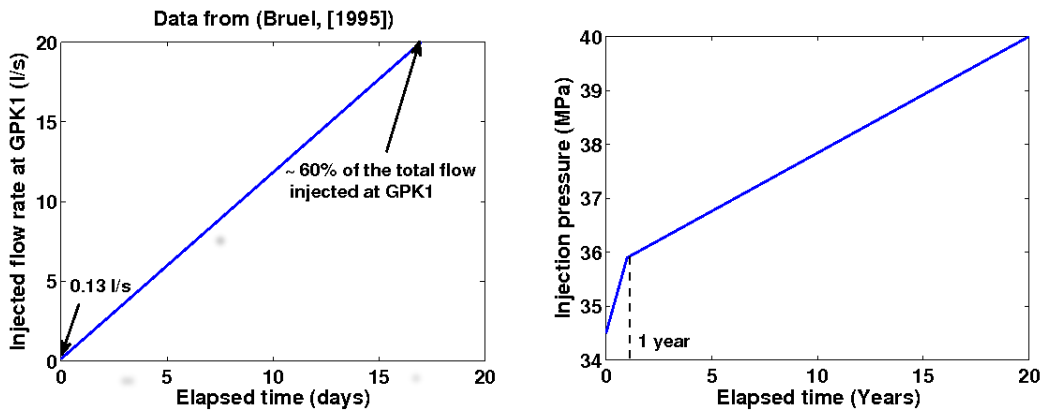


Figure 2: Injection conditions at GPK1 during the 1993 field injection test at Soultz-sous-Forêts (left) linear injection flow rate at early times, (right) time course of injection pressure at later times. The actual test includes injection at GPK1 well and production at two wells which are considered to be located symmetrically with respect to GPK1. Only a quarter of the reservoir is meshed.

When the reservoir is assumed impermeable at the outer and right boundaries (first scheme), the geothermal system reaches a pressure of 137 MPa at a flow rate 20 l/s with a plateau announcing the presence of extreme turbulent flow near GPK1, figure 3(left). This pressure of 137 MPa is 3.5 times higher than the HF pressure (40 MPa) deduced from Bruel [1995]₂. However, when the outer and right boundaries of the reservoir are assumed permeable (second scheme), the geothermal system reaches the pressure of HF at a flow rate of 20 l/s almost as applied experimentally. The numerical response in figure 3(right) is no longer showing an asymptotic plateau as the fluid turbulence is mostly eliminated when the outer and right boundaries are assumed permeable, i.e. smoother flow is achieved within the reservoir.

¹ The flow loss is approximately equal to 40%: the effective flow absorbed by the reservoir volume is about 60% of the total injected flow, i.e. 24 l/s. The value of 20 l/s is used in the simulations along Bruel [1995]₂, figure 2(left).

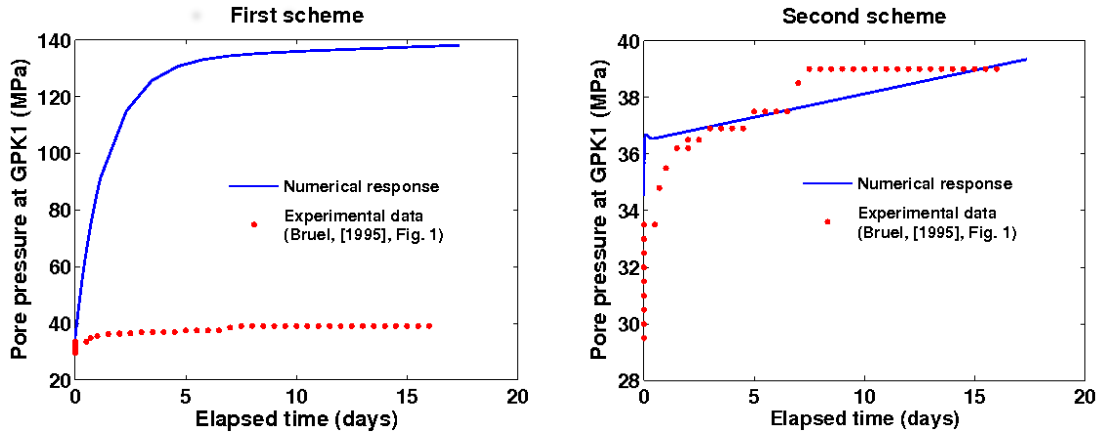


Figure 3: Injection pressure at GPK1 during the 1993 field injection test at Soultz-sous-Forêts: (left) impermeable boundaries; (right): permeable boundaries. Comparison between experimental data and the HFM responses for the two schemes sketched on Table 3.

5. HYDRAULIC FRACTURING, IMPEDANCE AND EFFICIENCY

While Section 4 was concerned with the early times of injection, the permeability enhancement over the whole reservoir is now addressed. The effects of HF process on the reservoir impedance and efficiency of thermal recovery are also presented during the life time of the reservoir. In order to highlight the qualitative and quantitative effects of HF, tests are run both with and without implementing the HF model (HFM). The finite element mesh includes 800 elements, 40 elements in x-direction and 20 elements in y-direction. Since focus is now on the volume of the reservoir rather than on the injection process, the mesh is uniformly spread over the volume.

The stability of the borehole GPK1 against shear failure has been checked previously. Injection pressure is increasing at GPK1 linearly: pumping starts with 34.5 MPa and reaches 35.9 MPa at year 1. Thereafter, it continues to increase also linearly but with a lower rate to reach a value of 40 MPa after 20 years of injection, figure 2(right). Regarding the hydraulic boundary conditions, the fluxes are now set to vanish on the four sides as the injection is controlled, no longer by the flow rate, but by the fluid pressure.

Convection of heat is treated a priori using the SUPG method, see e.g. Gelet [2011], Chap. 6. However, some stubborn numerical wiggles at the injection and production wells still require more attention as will be seen later in Section 5.2, see AbuAisha [2014], Chap. 6, for a detailed treatment of such noises.

5.1 Simulations on the natural reservoir without HF

The circulation tests on the natural (unenhanced) reservoir after 5 and 10 years of pumping are commented first.

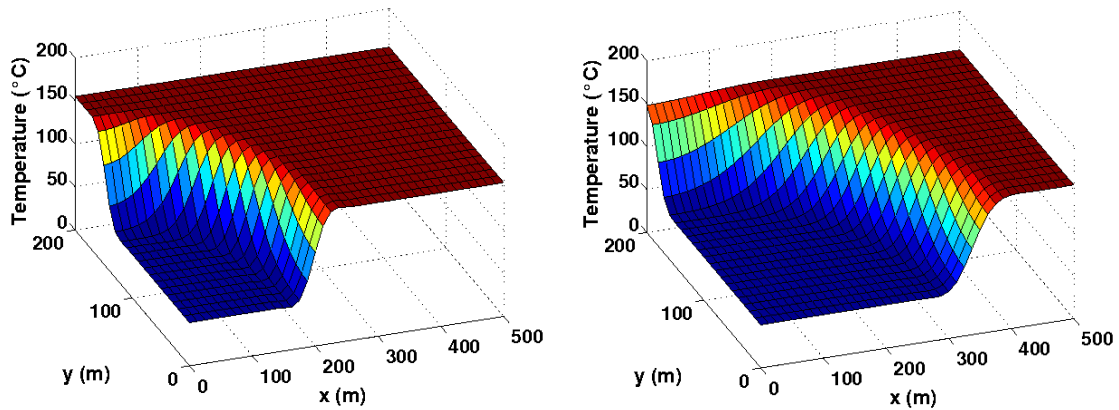


Figure 4: Contours of the temperature of the reservoir at year 5 (left) and year 10 (right); simulations without HF.

The pressure field has been established in the early times in a matter of days. Therefore the contours of fluid pore pressure are not showing any significant changes at later times. The reservoir cools in x- and y-directions, figure 4, due to the high fluid velocity spreading all over the volume of the reservoir.

The impedance Z , defined as the ratio of the pressure differential between the injection and production wells required to ensure the produced flow rate Q ,

$$Z = \frac{p_{inj} - p_{prod}}{Q} \tag{8}$$

is an important overall characteristic of a reservoir. The vertical section of the well GPK1, over which flow is taking place, is approximately 550 m extending to about 3.3 km and the radius of the well at such a depth is 15 cm, Baumgärtner et al. [2000]. Therefore, the flow takes place over an area of $\sim 518 \text{ m}^2$. Assuming no leak off, the impedance of the unenhanced reservoir on figure 5(right) can be obtained from the computed flux-pressure relation at the injection well GPK1 shown in figure 5(left). The time course of the injection pressure is shown on figure 2(right) and the production pressure is maintained at $p = p_0 - 1 = 27.5 \text{ MPa}$.

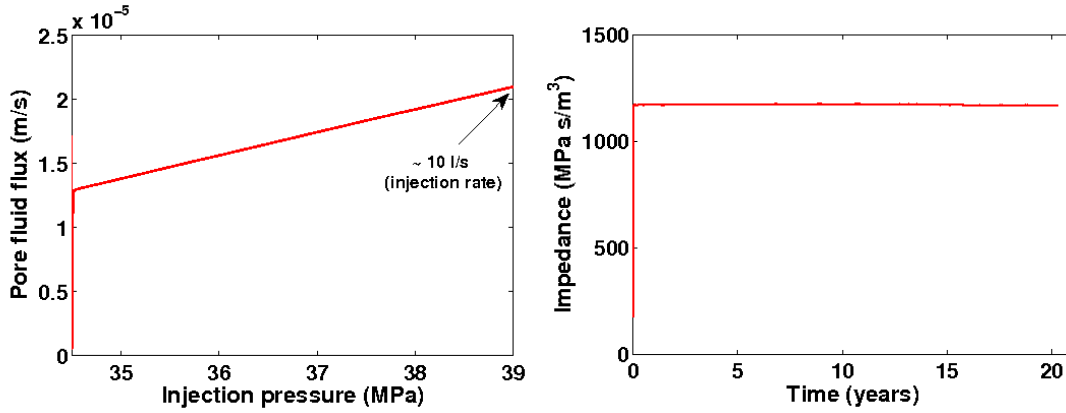


Figure 5: (left) Relation between injected pore fluid pressure and created fluid flux at the injection well GPK1 of unenhanced HDR reservoir at Soultz-sous-Forêts. The fluid flux increases linearly following the injection schedule shown on figure 2(right); (right) Impedance profile: an impedance greater than 1000 MPa/(m³/s) indicates inefficient operation.

Impedance is seen to be virtually constant in time and greater than 1000 MPa/(m³/s). Such a large impedance means an inefficient operation where the power pumped through the reservoir will most probably exceed a substantial fraction of the power produced by the reservoir, Murphy et al. [1999].

5.2 Simulations while implementing the HFM

When hydraulic fracturing is activated in our finite element code, cracks are evolving in the direction of maximum far field stress (along the x-axis) leading longitudinal permeability to reach its maximum value up to distances of $\sim 80 \text{ m}$ in y-direction and $\sim 240 \text{ m}$ in x-direction. The permeability contours for the enhanced HDR reservoir after 1 year of pumping at GPK1 are shown in figure 6. The results of this simulation are in good agreement with the micro-seismic events diagram presented in Bruel [1995]₂, Fig. 2, announcing the propagation of hydraulic front and fracture coalescence.

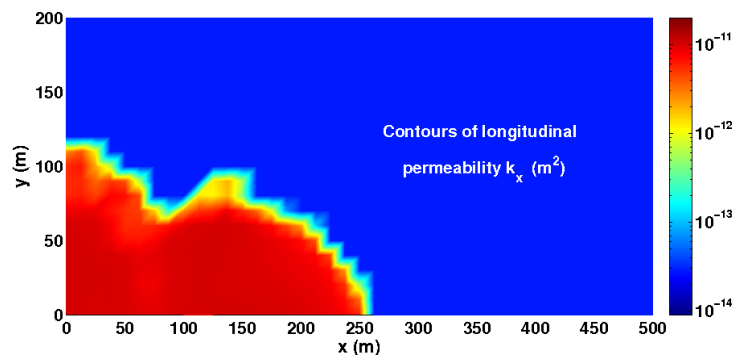


Figure 6: Contours of longitudinal permeability component $k_{xx} \text{ (m}^2\text{)}$ at year 1 of pumping; HF model is activated.

Preferential cooling following the new paths of the enhanced permeability is thus expected: heat convection is dominant in the direction of the major principal stress (direction of crack evolution), figure 7. The oscillations in temperature contours near the production well are related to the convection of heat as fluid fluxes converge leading to high pore fluid velocity. The Subgrid Scale method (SGS) and the Discontinuity Capturing Method (DCM) have been observed to be much more efficient to cure these oscillations than the SUPG method, AbuAisha [2014], Chap. 6.

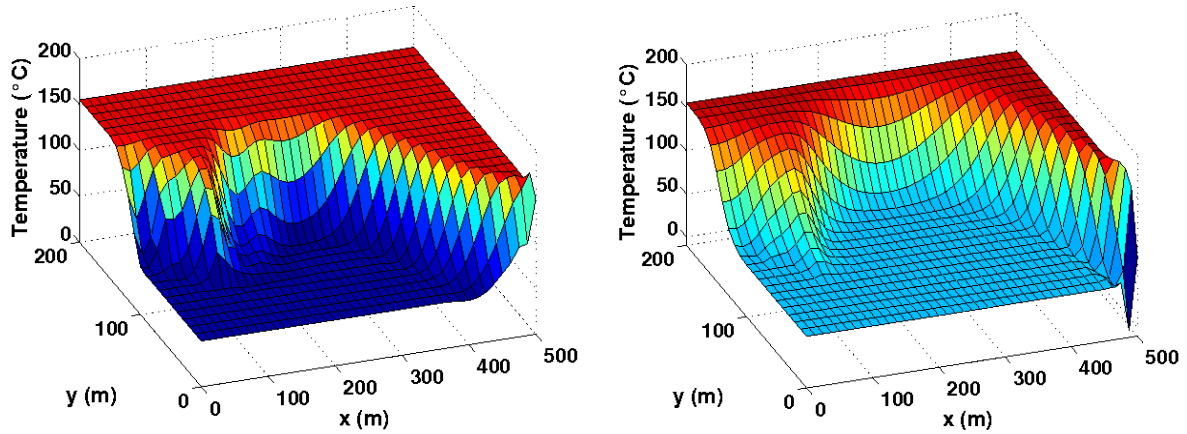


Figure 7: Contours of the reservoir temperature at year 5 (left) and year 10 (right); HF model is activated. Convection of heat is dominant in the direction of fracture evolution.

The velocity field at year 1 shows larger pore fluid velocity in the zone of active HF, about 2.75×10^{-5} m/s against 0.62×10^{-5} m/s in other regions.

The contours of pore fluid pressure at years 5 and 10 are shown in figure 8. The tremendous fast increase of the permeability in the zone of active HF makes the changes in pore fluid pressure quite small in this zone as compared to the situation of unenhanced HDR reservoir. This behavior of pressure distributions was also observed by Lee and Ghassemi [2010] for two-dimensional BVPs.

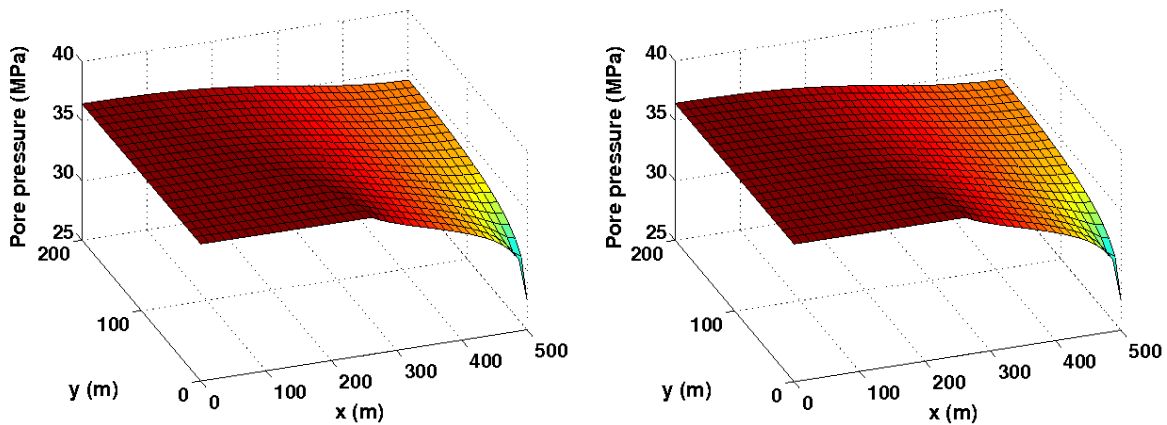


Figure 8: Contours of the reservoir pressure at year 5 (left) and year 10 (right); HF model is activated. The high permeability created by HF levels the pressure contours in the region of enhancement.

The contours of the longitudinal or transversal effective stresses, figures 9 and 10, follow the preferential cooling derived by the HF process. Stresses are dawkled in compression in the cooled regions as the reservoir is constrained to some degree on the boundaries of symmetry. The created new highly-permeable paths take most of the fluid velocity directly in the direction of maximum far field stress causing increased compressive stresses near the outer boundary of the HDR reservoir. Thus, at the outer boundary, cracks are most likely closing and permeability is decreasing, unless shear dilatation might cope for the reduction in their apertures. However, shear dilatation due to compressive stresses is not covered in this research.

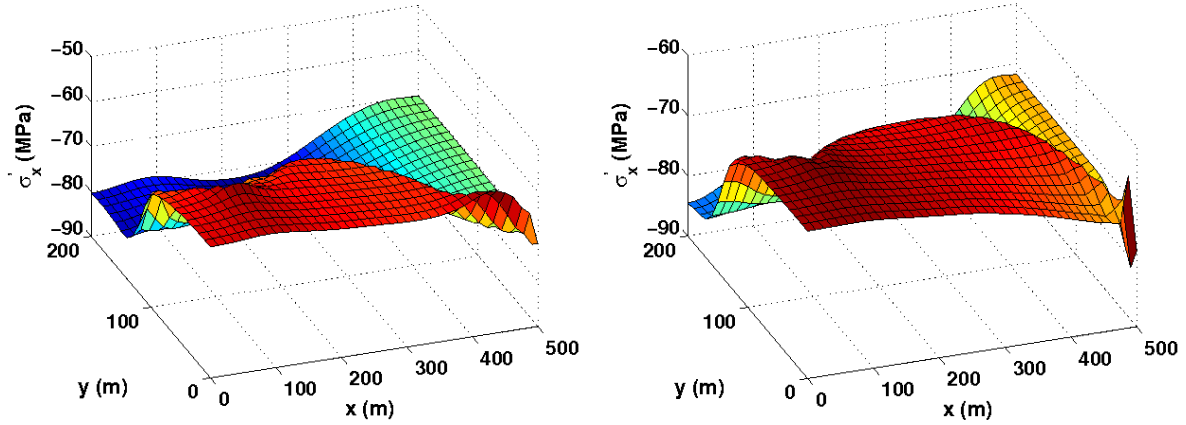


Figure 9: Contours of longitudinal effective stress σ'_{xx} at year 5 (left) and year 10 (right); HF model is activated. Stresses are dawdled in compression in the cooled regions due to tensile stresses.

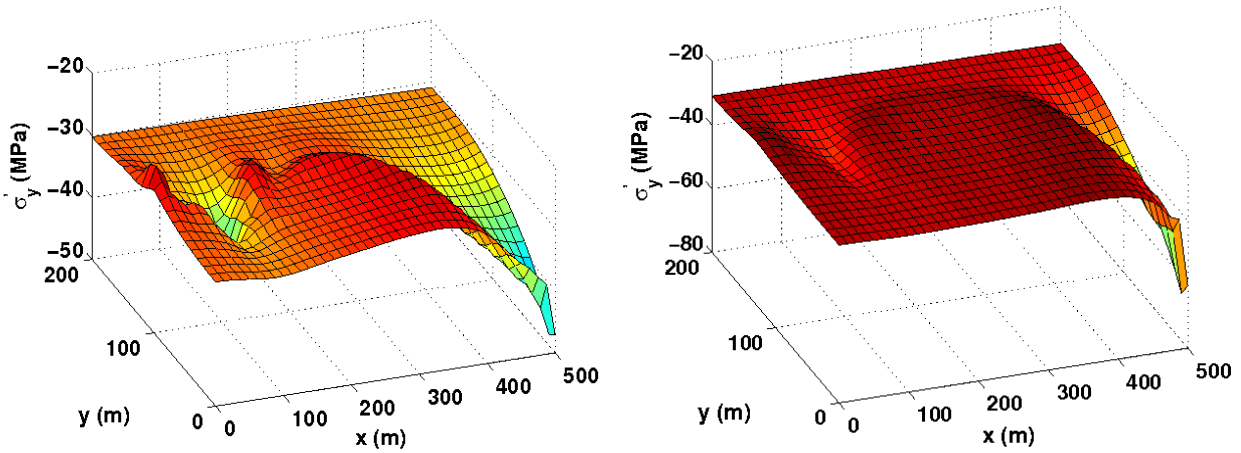


Figure 10: Contours of transversal effective stress σ'_{yy} at year 5 (left) and year 10 (right); HF model is activated.

The relation between injected pore fluid pressure and the ensuing fluid flux at the injection well GPK1 is non-linear during the first year of simulation while HF process is active, Figure 11(left). The non-linearity of the pressure-flow record witnesses the creation of improved connections around the borehole GPK1. It also describes the dependence of hydraulic conductivity on the effective stress. The statement of end of HF in figure 11(left) may sound puzzling. Actually, the experimental work of Papanastasiou [1999] suggests that, for every geothermal system, there exists an optimum injection schedule (injection pressure and duration). Any further increase in stimulation effort, i.e. stimulation time for a given stimulation pressure, does not provide additional permeability enhancement. Our injection pressure schedule defined in figure 2(right) was sufficient to enhance the reservoir permeability as shown in figure 6 up to year 1. The subsequent increase in stimulation pressure over time did not enhance the reservoir permeability any more. Therefore end of HF means the time and pressure values from which the enhancement of the reservoir is not operative any longer.

The jump between the two points M and N in figure 11 (left) can be explained by studying the permeability history at the injection well GPK1. The permeability evolution at the injection well happens very rapidly. This is due to modeling hydraulic fracturing while considering only mode I of fracture propagation. It is also seen that the period of intense permeability enhancement is taking place earlier at the injection well which is expected due to harsh thermo-poroelastic changes at this point. However, if permeability histories were averaged over the whole reservoir, the period of intense permeability enhancement in the averaged curve would correspond to the jump M-N in figure 11(left).

The process of HF, for only one year, has reduced the flow impedance of the HDR reservoir from about 1170 MPa/(m³/s) to 600 MPa/(m³/s), figure 11(right). This reduction in the impedance lowers the power required to pump water through the reservoir and enhances the efficiency by about 49%.

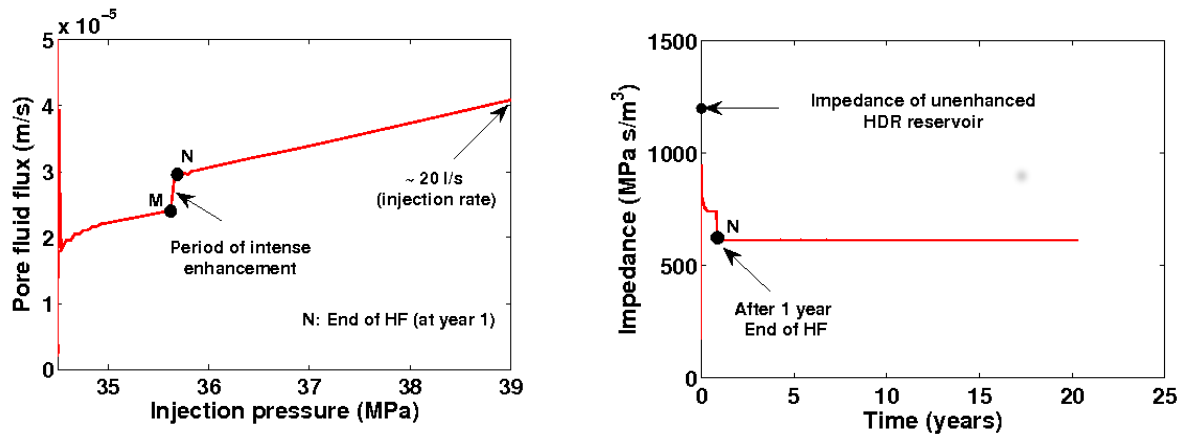


Figure 11: (left) Relation between injected pore fluid pressure and fluid flux at the injection well GPK1: non-linear relation results from the creation of improved connections; (right) Impedance profile of the enhanced HDR reservoir.

The profiles of fluid temperature at the production well with and without HF are compared in figure 12(left). In most geothermal systems, the produced fluid is efficiently used as long as its temperature does not drop below 80 °C. The standard mean production temperature curve, shown in figure 12 (left), is based on the analytical solution provided by Kolditz [1995], Fig. 5, for one-dimensional matrix heat diffusion and for 15 l/s injection flow rate.

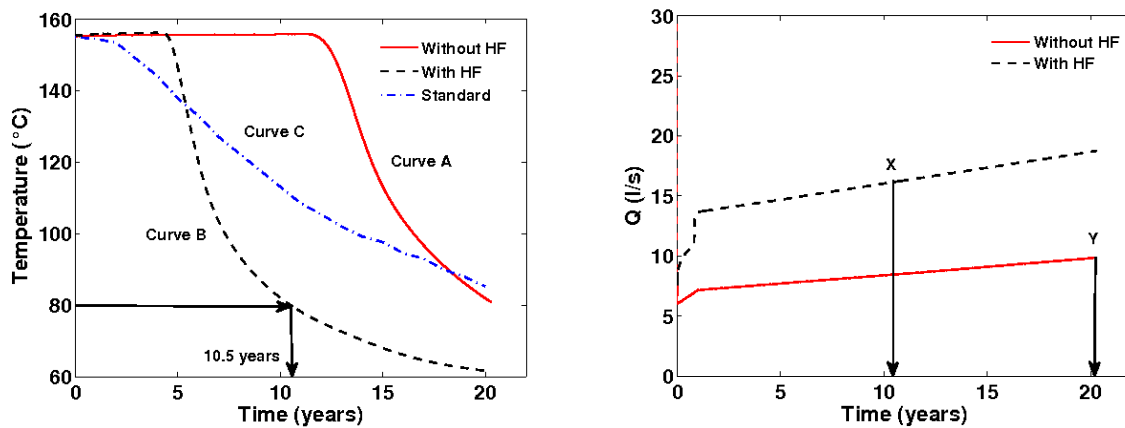


Figure 12: (left) Profiles of produced fluid temperature with HF and without HF; (right) Produced flow rate from the enhanced reservoir is two-fold the produced flow from the natural reservoir.

When the process of HF is utilized in the simulations, the HDR reservoir is exhausted in 10.5 years, figure 12(left). However, when HF is not activated, the HDR reservoir may last up to 20 years. Still, the efficiency of utilizing HF is evident in terms of the energy used to pump water through the reservoir, figure 11(right), and in terms of the produced flow rate, figure 12(right).

After 1 year of the process of HF, the produced flow rate from the HDR reservoir is 2 times higher than if the reservoir was not hydraulically stimulated. Considering that the stimulated reservoir will operate efficiently till 10.5 years and that the unenhanced reservoir will efficiently operate till 20 years, the volume of the produced fluid can be calculated by numerically integrating the curves, in figure 12(right), till point X for the case of active HF and point Y for the case of inactive HF: the volume of efficient fluid produced from the stimulated HDR reservoir over a period of 10.5 years is 4.922 Million m³, while the volume of efficient fluid produced from the unenhanced HDR reservoir over a period of 20 years is 5.364 Million m³. These huge amounts of water used are not utterly lost: the geothermal fluids are recirculated in a closed loop. It becomes clear now that HF process has increased the efficiency of the HDR reservoir up to 49% according to figure 11(right). Yet by the calculations of efficient fluid volume, only 7 to 8% of the total efficient fluid to be produced is lost over the entire effective age of the reservoir.

As another indicator of a geothermal reservoir, figure 13 shows the thermal drawdown of the enhanced HDR reservoir and the standard production curve as suggested by Kolditz [1995]. Thermal drawdown $T_D = 1 - T/T_0$ is defined as the relative difference between initial temperature of the reservoir T_0 and production temperature T . Kolditz standard solution shows a thermal drawdown of approximately 26% in 10 years, against 45% for the enhanced reservoir. In both cases, thermal drawdown exceeds the limits required by Jupe et al. [1995], namely 1% thermal drawdown per year. Still, this poor performance may be attributed for a part to the fact that the present heat diffusion analysis is two- rather than three-dimensional, Kolditz [1995].

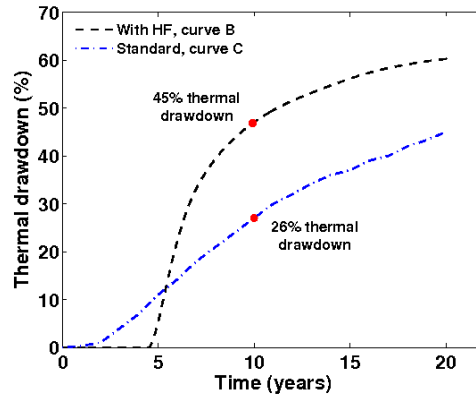


Figure 13: Thermal drawdown of the mean production temperature for the enhanced HDR reservoir curve B, and the standard production temperature as suggested by Kolditz [1995].

6. THE INFLUENCE OF WORKING FLUIDS IN GEOTHERMAL PROCESSES

Fluids usually used in geothermal systems are brines with the dominance of sodium chloride NaCl over a typical range of concentration. In most of the geothermal systems, as in Groß Schönebeck 50 km north of Berlin, the total of dissolved solids sums up to 265 g/l with a dominant mass fraction of 0.225 kg of NaCl per kg of solution corresponding to a molality of 4.968 mol of NaCl per kg of H₂O, Francke and Thorade [2010], Battistelli et al. [1997]. Francke and Thorade [2010] collected experimental data from several studies to provide three models to estimate brine viscosity temperature dependence. Figure 14 shows the viscosity of 0.225 kg of NaCl per kg of solution brine over a range of temperature of interest and at constant pressure of 1.5 MPa. The expression $\mu_b = 1.57 \times 10^{-3} \times (T/293)^{-4.37}$ Pa \times s, with T the temperature in Kelvin, is found to represent the average of the three models of Francke and Thorade with a determination coefficient of $R^2 = 0.9957$. Figure 14 also shows the viscosity of the water substance $\mu = 1.0 \times 10^{-3} \times 10^{247.8/(T-140)-1.62}$ Pa \times s as given by Burger et al. [1985]. At a temperature of 150 °C, the relative difference $\mu_b / \mu - 1$ as a result of using sodium chloride to a concentration of 0.225 kg NaCl /kg H₂O is equal to 65%.

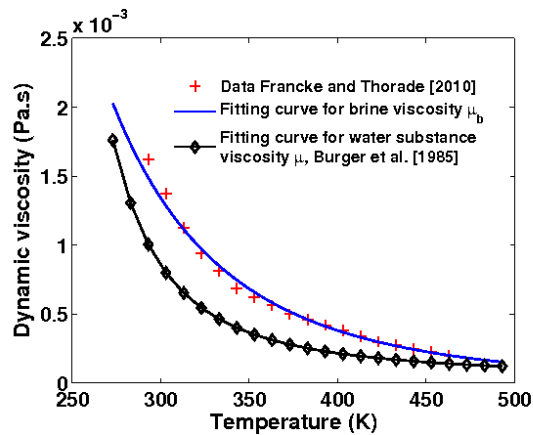


Figure 14: Viscosities of water and brine containing 0.225 kg of NaCl per kg of solution as a function of temperature at a constant pressure of 1.5 MPa.

The simulations with and without accounting for hydraulic fracturing of the stimulation tests of Section 3 have been re-run assuming brine as the working fluid. The pore fluid viscosity used in all the simulations presented in Section 3 corresponds to a temperature of 150 °C. Injecting cold brine at 50 °C is expected to increase brine viscosity μ_b by a threefold.

Increasing pore fluid viscosity definitely decreases the speed at which the hydraulic front is moving. Indeed, the pressure gradients with respect to the wells increase, so that the pore fluid pressure inside the reservoir decreases. This phenomenon can be observed on figure 15 that shows pore fluid pressure profiles along the line joining the wells GPK1 and GPK2. The reduction in pore fluid pressure as result of increasing brine viscosity shall definitely hinder the process of HF.

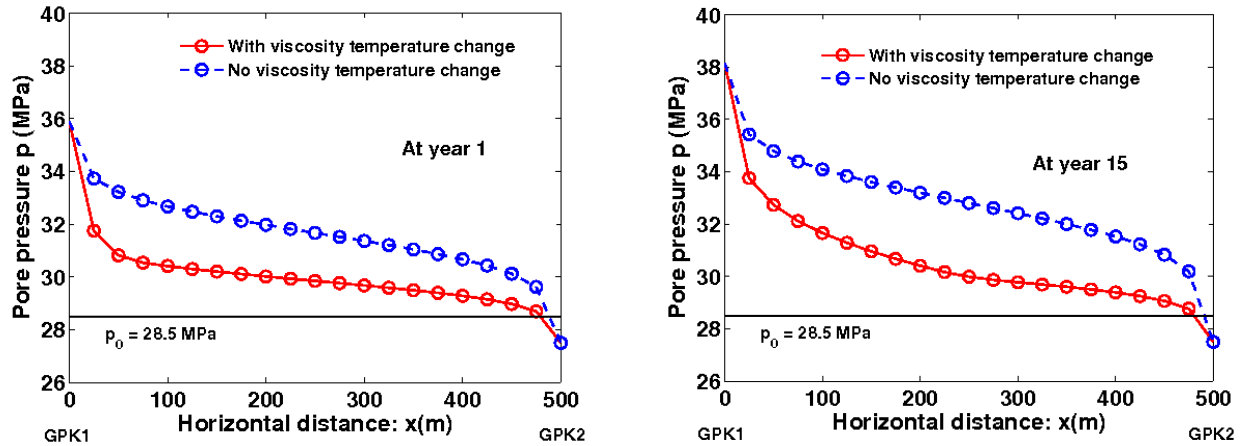


Figure 15: Pore pressure profiles along the line joining the injection and production wells, at year 1 and year 15. Solid lines: temperature-dependent viscosity; dashed lines: constant brine viscosity $\mu_b = 3 \times 10^{-4} \text{ Pa}\cdot\text{s}$.

REFERENCES

- AbuAisha, M.: Enhanced geothermal systems: Permeability stimulation through hydraulic fracturing in a thermo-poroelastic framework, PhD thesis, <https://tel.archives-ouvertes.fr/tel-01053612>, Université de Grenoble, France (April 2014).
- Atkinson, B. K.: Fracture mechanics of rock, second printing Edition, Academic Press Limited, London, Great Britain (1991).
- Battistelli, A., Calore, C., and Pruess, K.: The simulator TOUGH2 / EWASG for modelling geothermal reservoirs with brines and non-condensable gas, *Geothermics*, **26**(4), (1997), 437-464.
- Baumgärtner, J., Gérard, A., Baria, R., and Garnish, J.: Progress at the European HDR project at Soultz- sous-Forêts: Preliminary results from the deepening of the well GPK2 to 5000 m. *Proceedings, 25th Workshop on Geothermal Reservoir Engineering*, Stanford University, Stanford, California (22-24 January 2000).
- Bruel, D.: Heat extraction modelling from forced fluid flow through stimulated fractured rock masses: Application to the Rosemanowes hot dry rock reservoir, *Geothermics*, **24**(3), (1995)₁, 361-374.
- Bruel, D.: Modelling heat extraction from forced fluid flow through simulated fractured rock masses: Evaluation of the Soultz- sous-Forêts site potential, *Geothermics*, **24**(3), (1995)₂, 439-450.
- Burger, J., Sourieau, P., and Combarnous, M.: Thermal methods of oil recovery, Editions Technip, Paris (1985).
- Evans, K., Valley, B., Häring, M., Hopkirk, R., Baujard, C., Kohl, T., Megel, T., André, L., Portier, S., and Vuataz, F.: Studies and support for the EGS reservoirs at Soultz-sous-Forêts, Technical. report, Centre for Geothermal Research-CREGE, CHYN, University of Neuchâtel, (2009).
- Francke, H. and Thorade, M.: Density and viscosity of brine: An overview from a process engineers perspective, *Chemie der Erde*, **70**(S3), (2010), 23-32.
- Gelet, R.: Thermo-hydro-mechanics of deformable porous media with double porosity and local thermal non-equilibrium, PhD thesis, <https://tel.archives-ouvertes.fr/tel-00712459>, Université de Grenoble, France (September 2011).
- Jupe, A. J., Bruel, D., Hicks, T., Hopkirk, R., Kappelmeyer, O., Kohl, T., Kolditz, O., Rodrigues, N., Smolka, K., Willis-Richards, J., Wallroth, T., and Xu, S.: Modelling of a European prototype HDR reservoir, *Geothermics*, **24**(3), (1995), 403-419.
- Kolditz, O.: Modelling flow and heat transfer in fractured rocks: Dimensional effect of matrix heat diffusion, *Geothermics*, **24**(3), (1995) 421-437.
- Lee, S. H., and Ghassemi, A.: Thermo-poroelastic analysis of injection-induced rock deformation and damage evolution, *Proceedings, 35th Workshop on Geothermal Reservoir Engineering*, Stanford University, Stanford, California, 2010.
- Murphy, H., Brown, D., Jung, R., Matsunaga, I., and Parker, R.: Hydraulics and well testing of engineered geothermal reservoirs, *Geothermics*, **28**, (1999), 491-506.
- Papanastasiou, P.: The effective fracture toughness in hydraulic fracturing, *International Journal of Fracture*, **96**, (1999), 127-147.
- Shao, J. F., Zhou, H., and Chau, K. T.: Coupling between anisotropic damage and permeability variation in brittle rocks, *International Journal for Numerical and Analytical Methods in Geomechanics*, **29**, (2005), 1231-1247.